Composite Structures 106 (2013) 317–325

Contents lists available at SciVerse ScienceDirect

Composite Structures

journal homepage: www.elsevier.com/locate/compstruct

Free vibration analysis of rotating composite blades via Carrera Unified Formulation

E. Carrera [a,b], M. Filippi [a,*], E. Zappino [a]

[a] Department of Mechanical and Aerospace Engineering, Politecnico di Torino, Corso Duca degli Abruzzi 24, 10129 Torino, Italy
[b] King Abdulaziz University, Jeddah, Saudi Arabi

ARTICLE INFO

Article history:
Available online 22 June 2013

Keywords:
Rotating beams
Finite Element Method
Higher-order theories
Composites structures

ABSTRACT

Carrera Unified Formulation (CUF) is used to perform free-vibrational analyses of rotating structures. CUF is a hierarchical formulation which offers a procedure to obtain refined structural theories that account for variable kinematic description. These theories are obtained by expanding the unknown displacement variables over the beam section axes by adopting Taylor's expansions of N-order, in which N is a free parameter. Linear case ($N = 1$) permits us to obtain classical beam theories while higher order expansions can lead to three-dimensional description of dynamic response of blades. The Finite Element Method is used to solve the governing equations of rotating blades that are derived in a weak form by means of Hamilton's Principle. These equations are written in terms of "fundamental nuclei", which do not vary with the theory order (N). Both flapwise and lagwise motions of isotropic, composite and thin-walled structures are traced. The Coriolis force field is included in the equations. Results are presented in terms of natural frequencies and comparisons with published solutions are provided.

1. Introduction

A thorough understanding of the dynamic features of rotating blades serves as a starting point for the study of fatigue effects, forced-response and flutter instability, which occur in airplane engines, helicopters and turbomachinery. Rotating structures where a geometrical dimension is predominant over the others are usually modeled as beams. Many researchers have addressed the problem of the rotating beam by simplifying both the equations of motion and the displacement formulations. For instance, Banerjee [1,2], Ozge and Kaya [3], Mei [4] and Hodges and Rutkowski [5] limited their studies to the flexural vibrations of both uniform and tapered Euler–Bernoulli rotating beams by using, respectively, the Dynamic Stiffness Method, the Differential Transform Method and a variable-order finite element. The assumption that the beam deforms only in bending is restrictive, since the coupling between the axial deformation and the lagwise motion can be significant. In order to take into account this coupling the introduction of the Coriolis force becomes mandatory. For this reason, Hsiao et al. solved the complete motion equations of Euler beams by using the power series solution [6] and the Finite Element Method [7]. Further improvements have been introduced by introducing enhanced displacement fields over the blade cross-section. Indeed, in the open literature, there are many papers devoted to the development of theories for the rotating structures based on the Timoshenko model, in which the Coriolis term has [8] or has not been considered [9–12]. In all papers mentioned, the generic rotating blade is assumed to be a compact structure constituted by isotropic material or by orthotropic laminae. However, the design of advanced rotor blades has been strongly affected by the advent of composite materials which combine a high specific strength and stiffness with the capability to be easily modeled. These properties produce light and efficient blades, whose dynamic characteristics usually involve phenomena that cannot be detected by the use of the classical models. For this reason, a considerable number of refined theories have been introduced with the purpose of describing the rotating composite blade behavior. For instance, Song and Librescu presented in [13] a structural model encompassing transverse shear, secondary warping deriving from the assumption of the non-uniform torsion along the longitudinal axis and the effect of the heterogeneity of the materials. They observed that by discarding the Coriolis term, the equations described separately the flap-lag deformation and the extension-twist motion, and within this context, they examined the ply orientation effects. Contrary to this ad hoc formulation, Chandiramani et al. provided a geometrically nonlinear theory for analyzing the rotating composite thin-walled box beam [14], in which the non-classical effects were captured in a general way. The linearized equations of motion were solved with the Modified Galerkin Method and the Coriolis term was disregarded. Furthermore, the authors modified their formulation for extension to pre-twisted composite blades [15]. See [16,17], for interesting studies on controlling thin-walled

* Corresponding author. Tel.: +39 011 090 6870.
E-mail addresses: erasmo.carrera@polito.it (E. Carrera), matteo.filippi@polito.it (M. Filippi), enrico.zappino@polito.it (E. Zappino).

0263-8223/$ - see front matter © 2013 Elsevier Ltd. All rights reserved.
http://dx.doi.org/10.1016/j.compstruct.2013.05.055

composite blades via piezoelectric patches. Jung et al. [18] developed a one-dimensional finite element based on a mixed variational approach in which both displacement and force formulations were used. The walls of the considered structures were modeled as shell and the global deformation was described by the Timoshenko beam model. This model is suitable for composite structures with open and closed contour. The dynamic of the rotating composite blades clearly represents a complex and interesting topic (see [19,20]), but it seems that a reliable and general method for its complete analysis is not yet available. In order to overcome the limitation of *ad-hoc* assumptions about the displacement fields, this paper presents the Carrera Unified Formulation (CUF). First of all, CUF offers a procedure to obtain refined structural models by considering the order and the types of theories as free input parameters, hence nonclassical effects such as warping, coupling, and torsion, are captured by simply enriching the displacement fields. Secondly, by using the Finite Element Method, it is possible to solve complete equations of motion by including the Coriolis term and both Stiffness and Softening centrifugal contributions. CUF was first developed for plate and shell models [21–25] and was later extended to the beam model [26]. The refined displacement fields are written adopting N-order Taylor type expansions (TE) [27] of the section coordinates. The refined finite elements have been evaluated in static and dynamic analyses carried out on unconventional cross-sections (hollow cylindrical reinforced structures, airfoil, bridge-like cross-sections, etc.) in [28–35]. As far as composite beams are concerned, interesting analyses are presented in [36–39]. Many other papers devoted to CUF are available in the literature but, for a thorough and clear description, see [26].

2. The kinetic and potential energies

When a structure is rotating, inertial forces and moments are observed. In this study, a beam that is free to rotate about one of its transverse axes with a constant spin-speed Ω is considered. Fig. 1 shows the reference frame of the beam. The absolute velocity of the point P is the sum of the relative velocity and the transfer velocity.

$$\boldsymbol{v}_{abs} = \boldsymbol{v}_{rel} + \boldsymbol{v}_{tr} = \dot{\boldsymbol{u}} + \boldsymbol{\Omega} \times \boldsymbol{r}_{\boldsymbol{tot}} \tag{1}$$

$$\boldsymbol{\Omega} = \begin{bmatrix} 0 & -\Omega & 0 \\ \Omega & 0 & 0 \\ 0 & 0 & 0 \end{bmatrix}$$

where $\boldsymbol{u}=\{u_x\ u_y\ u_z\}^T$ is the displacement vector, $\boldsymbol{r}_{\boldsymbol{tot}} = \boldsymbol{r} + \boldsymbol{u}$ is the distance of P from the neutral axis and the dot indicates the time derivative. The kinetic energy of the whole structure can be written as the following expression:

$$T = \frac{1}{2}\int_V \rho(\dot{\boldsymbol{u}}^T\dot{\boldsymbol{u}} + 2\boldsymbol{u}^T\boldsymbol{\Omega}^T\dot{\boldsymbol{u}} + \boldsymbol{u}^T\boldsymbol{\Omega}^T\boldsymbol{\Omega}\boldsymbol{u} + 2\dot{\boldsymbol{u}}^T\boldsymbol{\Omega}\boldsymbol{r} + 2\boldsymbol{u}^T\boldsymbol{\Omega}^T\boldsymbol{\Omega}\boldsymbol{r})dV \tag{2}$$

where ρ is the density of the structure. In order to take into account that the body can be loaded by static stresses, such as the centrifugal stress σ_0, in accordance with the linearized theory, the potential energy can be written in the following form:

$$U = \frac{1}{2}\int_V (\boldsymbol{\epsilon}_l^T\boldsymbol{C}\boldsymbol{\epsilon}_l)dV + \int_V (\boldsymbol{\sigma}_0{}^T\boldsymbol{\epsilon}_{nl})dV \tag{3}$$

where $\boldsymbol{\epsilon}_l$ and $\boldsymbol{\epsilon}_{nl}$ are the linear and nonlinear components of the strain field and $\boldsymbol{C}$ is the matrix of material coefficients. In the case in point, the tension due to centrifugal effect is:

$$\sigma_0 = \Omega^2\rho\left[r_hL + \frac{1}{2}L^2 - r_hy - \frac{1}{2}y^2\right] \tag{4}$$

where L and r_h are the length of the beam and the dimension of the hub.

3. The unified formulation

The CUF states that the displacement field, $\boldsymbol{u}(x,y,z,t)$, is an expansion of generic functions, $F_\tau(x,z)$ for the vector displacement, $\boldsymbol{u}_\tau(y)$:

$$\boldsymbol{u}(x,y,z,t) = F_\tau(x,z)\boldsymbol{u}_\tau(y,t) \qquad \tau = 1,2,\ldots,T \tag{5}$$

where T is the number of terms of the expansion and, in according to the generalized Einstein's notation, τ indicates summation. In this work, functions F_τ in Eq. (5) are Taylor-like expansions. For example, the second-order displacement field is:

$$\begin{aligned} u_x &= u_{x_1} + x\,u_{x_2} + z\,u_{x_3} + x^2\,u_{x_4} + xz\,u_{x_5} + z^2\,u_{x_6} \\ u_y &= u_{y_1} + x\,u_{y_2} + z\,u_{y_3} + x^2\,u_{y_4} + xz\,u_{y_5} + z^2\,u_{y_6} \\ u_z &= u_{z_1} + x\,u_{z_2} + z\,u_{z_3} + x^2\,u_{z_4} + xz\,u_{z_5} + z^2\,u_{z_6} \end{aligned} \tag{6}$$

while the third-order displacement field becomes:

$$\begin{aligned} u_x &= u_{x_1} + x\,u_{x_2} + z\,u_{x_3} + x^2\,u_{x_4} + xz\,u_{x_5} + z^2\,u_{x_6} + x^3\,u_{x_7} + x^2z\,u_{x_8} + xz^2\,u_{x_9} + z^3\,u_{x_{10}} \\ u_y &= u_{y_1} + x\,u_{y_2} + z\,u_{y_3} + x^2\,u_{y_4} + xz\,u_{y_5} + z^2\,u_{y_6} + x^3\,u_{y_7} + x^2z\,u_{y_8} + xz^2\,u_{y_9} + z^3\,u_{y_{10}} \\ u_z &= u_{z_1} + x\,u_{z_2} + z\,u_{z_3} + x^2\,u_{z_4} + xz\,u_{z_5} + z^2\,u_{z_6} + x^3\,u_{z_7} + x^2z\,u_{z_8} + xz^2\,u_{z_9} + z^3\,u_{z_{10}} \end{aligned} \tag{7}$$

A remarkable feature is that classical beam theories are obtainable as particular cases of Taylor expansions. It should be noted that classical theories require reduced material stiffness coefficients to contrast Poisson's locking. Unless otherwise specified, for classical

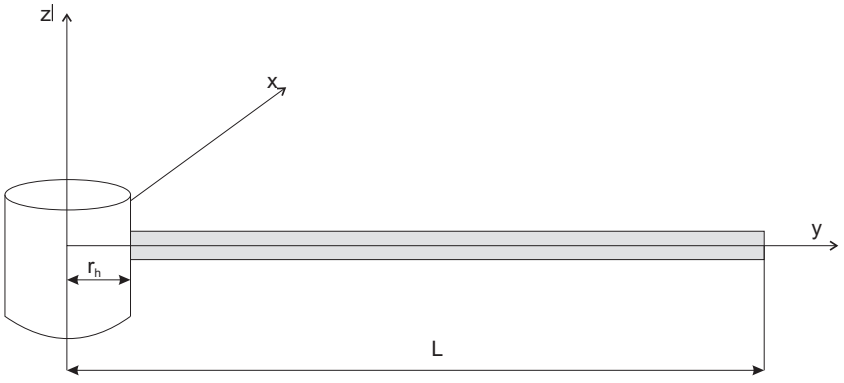

Fig. 1. Reference system.

and first-order models Poisson's locking is corrected according to Carrera et al. [26].

If a classical Finite Element technique is adopted with the purpose of easily dealing with arbitrary lamination schemes and generic boundary conditions, the generalized displacement vector becomes:

$$\mathbf{u}_\tau(y) = N_i(y)\mathbf{q}_{\tau i}(t) \tag{8}$$

where $N_i(y)$ are the shape functions and $\mathbf{q}_{\tau i}(t)$ is the nodal displacement vector:

$$\mathbf{q}_{\tau i}(t) = \left\{ q_{u_{x_{\tau i}}} \quad q_{u_{y_{\tau i}}} \quad q_{u_{z_{\tau i}}} \right\}^T \tag{9}$$

4. Equations of motion in CUF form

In order to obtain the motion equations, Hamilton's principle is used, and in the usual form it states:

$$\delta \int_{t_0}^{t_1} (T - U)\, dt = 0 \tag{10}$$

where δ is the virtual variation of the functional.

The assumptions made in the above section allow us to rewrite Eq. (10) as follow:

$$\int_{t_0}^{t_1} \left(\delta \boldsymbol{q}_{\tau i}^T \boldsymbol{M}^{ij\tau s} \ddot{\boldsymbol{q}}_{sj} + \delta \boldsymbol{q}_{\tau i}^T \boldsymbol{G}^{ij\tau s} \dot{\boldsymbol{q}}_{sj} + \delta \boldsymbol{q}_{\tau i}^T \left(\boldsymbol{K}^{ij\tau s} - \boldsymbol{K}_{\boldsymbol{\Omega}}^{ij\tau s} + \boldsymbol{K}_{\boldsymbol{\sigma_0}}^{ij\tau s} \right) \boldsymbol{q}_{sj} + \delta \boldsymbol{q}_{\tau i}^T \boldsymbol{F}_{\boldsymbol{\Omega}}^{i\tau} \boldsymbol{r} \right) dt = 0 \tag{11}$$

The matrices are written in form of the fundamental nuclei and their explicit forms are:

$$\begin{aligned}
\boldsymbol{M}^{ij\tau s} &= I_l^{ij} \lhd (F_\tau \rho \boldsymbol{I} F_s) \rhd \\
\boldsymbol{G}^{ij\tau s} &= I_l^{ij} \lhd (F_\tau \rho \boldsymbol{I} F_s) \rhd 2\boldsymbol{\Omega} \\
\boldsymbol{K}_{\Omega}^{ij\tau s} &= I_l^{ij} \lhd (F_\tau \rho \boldsymbol{I} F_s) \rhd \boldsymbol{\Omega}^T \boldsymbol{\Omega} \\
\boldsymbol{K}_{\sigma_0}^{ij\tau s} &= I_{l\sigma_0}^{i,yj,y} \lhd (F_\tau \rho \boldsymbol{I} F_s) \rhd \boldsymbol{\Omega}^T \boldsymbol{\Omega} \\
\boldsymbol{K}^{ij\tau s} &= I_l^{ij} \lhd \boldsymbol{D}_{np}^T (F_\tau \boldsymbol{I}) [\boldsymbol{C}_{np} \boldsymbol{D}_p (F_s \boldsymbol{I}) + \boldsymbol{C}_{nn} \boldsymbol{D}_{np} (F_s \boldsymbol{I})] \\
&\quad + \boldsymbol{D}_p^T (F_\tau \boldsymbol{I}) [\boldsymbol{C}_{pp} \boldsymbol{D}_p (F_s \boldsymbol{I}) + \boldsymbol{C}_{pn} \boldsymbol{D}_{np} (F_s \boldsymbol{I})] \rhd \\
&\quad + I_l^{ij,y} \lhd \left[\boldsymbol{D}_{np}^T (F_\tau \boldsymbol{I}) + \boldsymbol{D}_p^T (F_\tau \boldsymbol{I}) \boldsymbol{C}_{pn} \right] F_s \rhd + \boldsymbol{I}_{\Omega y} \\
&\quad + I_l^{i,yj} \boldsymbol{I}_{\Omega y}^T \lhd F_\tau [\boldsymbol{C}_{np} \boldsymbol{D}_p (F_s \boldsymbol{I}) + \boldsymbol{C}_{nn} \boldsymbol{D}_{np} (F_s \boldsymbol{I})] \rhd \\
&\quad + I_l^{i,yj,y} \boldsymbol{I}_{\Omega y}^T \boldsymbol{I}_{\Omega y} \lhd F_\tau \boldsymbol{C}_{nn} F_s \rhd \\
\boldsymbol{F}_{\Omega}^{i\tau} &= I_l^i \lhd F_\tau \rho \boldsymbol{r} \rhd \boldsymbol{\Omega}^T \boldsymbol{\Omega}
\end{aligned} \tag{12}$$

where:

$$\boldsymbol{I}_{\Omega\, y} = \begin{bmatrix} 0 & 0 & 1 \\ 1 & 0 & 0 \\ 0 & 1 & 0 \end{bmatrix} \qquad \lhd \ \ldots \ \rhd_\Omega = \int_\Omega \ldots \, d\Omega \tag{13}$$

$$\left(I_l^i,\, I_l^{ij},\, I_l^{ij,y},\, I_l^{i,yj},\, I_l^{i,yj,y},\, I_{l\sigma_0}^{i,yj,y} \right) = \int_l (N_i, N_i N_j,\, N_i N_{j,y},\, N_{i,y} N_j,\, N_{i,y} N_{j,y},\, \sigma_0 N_{i,y} N_{j,y})\, dy \tag{14}$$

In addition to the Mass Matrix $\boldsymbol{M}^{ij\tau s}$ and the Stiffness Matrix $\boldsymbol{K}^{ij\tau s}$ the expression of the kinetic energy introduces other three terms:

- the Coriolis Matrix $\boldsymbol{G}^{ij\tau s}$
- the Centrifugal Softening Matrix $\boldsymbol{K}_{\Omega}^{ij\tau s}$
- the Centrifugal Stiffening Matrix $\boldsymbol{K}_{\sigma_0}^{ij\tau s}$
- the Load vector $\boldsymbol{F}_{\Omega}^{i\tau}$

To obtain the natural frequencies and the normal modes of the rotor, we have to solve the homogeneous equations:

$$\boldsymbol{M}\ddot{\boldsymbol{q}} + \boldsymbol{G}_\Omega \dot{\boldsymbol{q}} + (\boldsymbol{K} - \boldsymbol{K}_\Omega + \boldsymbol{K}_{\sigma_0})\boldsymbol{q} = 0 \tag{15}$$

Now, it is possible to assume a periodic function as solution:

$$\boldsymbol{q} = \bar{\boldsymbol{q}} e^{i\omega t} \tag{16}$$

where $\bar{q}$ is the amplitude vector of the motion, 'i' is the imaginary unit and ω the circular or angular frequency. Substituting Eq. (16) and its derivative in Eq. (15), it becomes:

$$\bar{\boldsymbol{q}} e^{i\omega t} [(\boldsymbol{K} - \boldsymbol{K}_\Omega + \boldsymbol{K}_{\sigma_0}) + (\boldsymbol{G}_\Omega) i\omega - (\boldsymbol{M})\omega^2] = 0 \tag{17}$$

5. Numerical results

In order to assess the theory proposed, several illustrative examples are presented. The boundary conditions and the beam dimensions are assumed to be problem parameters. With the purpose of enabling a general application of results, if not otherwise declared, they are presented in non-dimensional form by adopting the following expressions:

Table 1
Dependency of the first three dimensionless natural frequency parameters on the variations of the dimensionless angular speed and hub dimension of a Euler–Bernoulli beam.

B.C.	ω^*	Theory	$\Omega^* = 1$		$\Omega^* = 5$	
			$\delta_t = 0$	$\delta_t = 1$	$\delta_t = 2$	$\delta_t = 3$
$C-F$	1	[1]	3.6816	3.8888	10.862	12.483
		Present	3.6816	3.8895	10.866	12.488
	2	[1]	22.181	22.375	32.764	35.827
		Present	22.178	22.375	32.773	35.840
	3	[1]	61.842	62.043	73.984	77.935
		Present	61.836	62.032	73.986	77.939
$C-P$	1	[1]	15.513	15.650	22.663	24.729
		Present	15.512	15.649	22.670	24.738
	2	[1]	50.093	50.277	60.906	64.382
		Present	50.092	50.275	60.919	64.399
	3	[1]	104.39	104.59	116.99	121.30
		Present	104.42	104.62	117.04	121.36
$P-P$	1	[1]	10.022	10.264	19.684	22.078
		Present	10.021	10.264	19.690	22.086
	2	[1]	39.642	39.889	53.132	57.235
		Present	39.638	39.886	53.141	57.248
	3	[1]	88.991	89.241	103.92	108.93
		Present	89.003	89.253	103.94	108.96

Table 2
Non-dimensional fundamental frequency ω^* of a cantilever Timoshenko beam as a function of the rotating speed.

Ω^*	[9]	Present	*Diff.* (%)
0	3.4798	3.4831	0.09
1	3.6452	3.6494	0.11
2	4.0994	4.1064	0.17
3	4.7558	4.7667	0.22
4	5.5375	5.5530	0.27
5	6.3934	6.4144	0.32
6	7.2929	7.3205	0.37
7	8.2184	8.2538	0.43
8	9.1596	9.2039	0.48
9	10.109	10.164	0.54

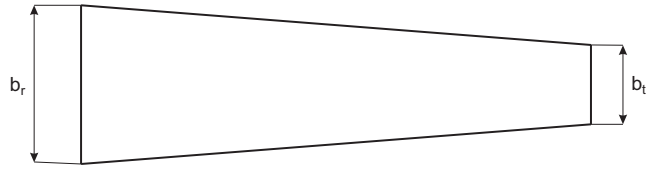

Fig. 2. Tapered Beam.

Table 3
Dependency of the first three dimensionless natural frequency parameters on the variations of the dimensionless angular speed for uniform ($\delta_t = 1$) and tapered ($\delta_t = 0$) beams.

Ω^*	ω^*	Uniform			Tapered		
		[5]	Present	Diff. (%)	[5]	Present	Diff. (%)
0	1	3.5160	3.5164	0.01	3.8237	3.8569	0.87
	2	22.034	22.034	0.00	18.317	18.375	0.31
	3	61.697	61.685	0.02	47.264	47.442	0.38
1	1	3.8888	3.8895	0.18	3.9866	4.0505	1.60
	2	22.375	22.375	0.00	18.474	18.559	0.46
	3	62.043	62.032	0.02	47.417	47.625	0.32
5	1	8.9403	8.9443	0.04	6.7344	7.2335	7.41
	2	29.352	29.360	0.03	21.905	22.538	2.89
	3	69.760	69.772	0.17	50.933	51.821	1.74
10	1	16.606	16.615	0.05	11.501	12.638	9.88
	2	44.368	44.384	0.04	30.182	31.857	5.55
	3	89.156	89.169	0.01	60.564	63.043	4.09

$$\omega^* = \frac{\omega}{\omega_0}, \qquad \Omega^* = \frac{\Omega}{\omega_0}, \qquad \omega_0 = \sqrt{\frac{\rho A L^4}{E J_{xx}}} \qquad \delta_t = \frac{r_h}{L}$$

$$S = \sqrt{\frac{AL^2}{J_{xx}}}$$

Table 4
Dependency of the first dimensionless fundamental frequency parameter on the variations of the dimensionless angular speed and hub dimension for the chordwise motion.

δ_t	Ω^*	Present	[40]	Diff. (%)
0	2	3.6196	3.6173	0.06
	10	4.9700	4.9619	0.16
	50	7.3337	7.4537	1.63
1	2	4.3978	4.3960	0.04
	10	13.048	13.047	0.01
	50	41.227	41.346	0.28
5	2	6.6430	6.6421	0.01
	10	27.266	27.276	0.03
	50	74.003	74.178	0.23

where J_{xx} is the moment of inertia about x-axis, E is the Young Modulus and A the area of the cross-section. In the first test case, a thin rotating beam is considered and the non-dimensional results obtained in CUF form are compared with those presented in [1] in which the Dynamic Stiffness Method were employed. As can be seen in Table 1, the results are in strong agreement with the reference for all kinds of boundary conditions (B.C.) and for the considered hub off-set ratios. The boundary conditions

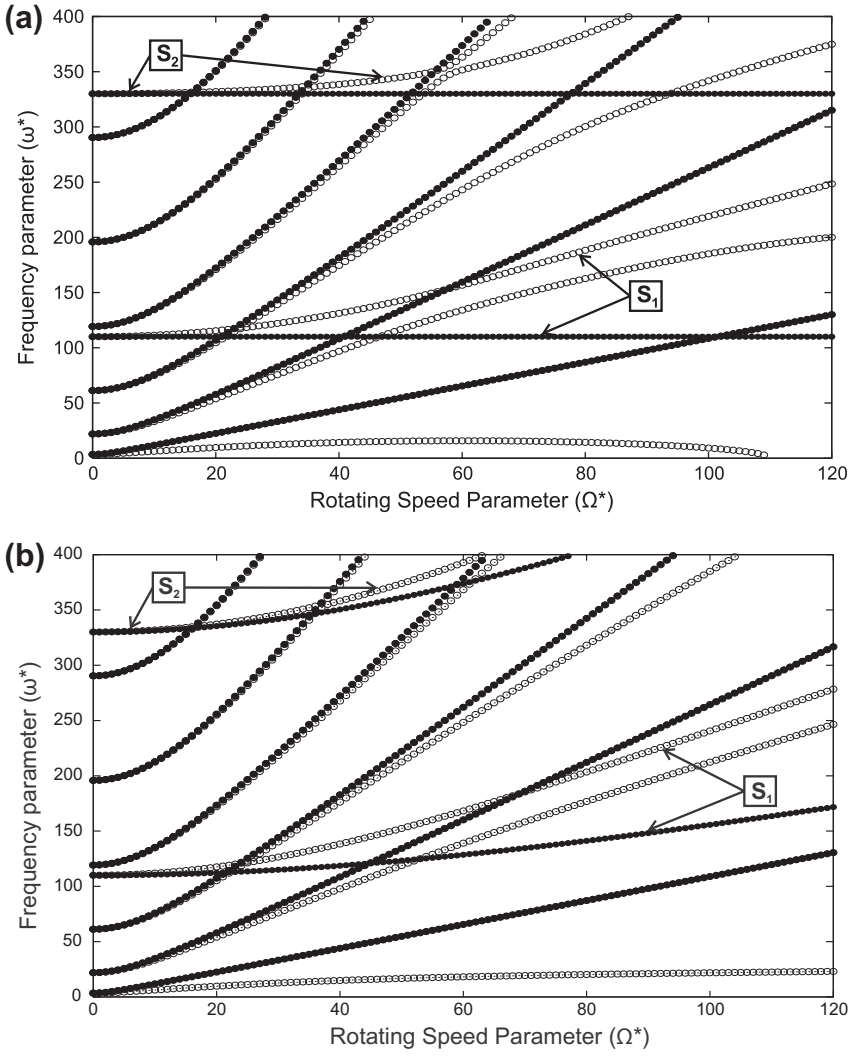

Fig. 3. Variation of the non-dimension natural frequencies for the speed parameter when $\delta = 0.1$ and $S = 70$ – "•": flapwise motion and "○": chordwise motion.

Table 5
Material and dimensions of graphite-epoxy beams.

Case	Thickness (mm)	Orientation (°)
1	2.97	0
2	3.22	15
Property	Dimension (GPa)	
E_{11}	141.9	
$E_{22} = E_{33}$	9.780	
$G_{21} = G_{31}$	6.140	
G_{32}	5.520	
$\nu_{12} = \nu_{13}$	0.42	
ν_{23}	0.54	

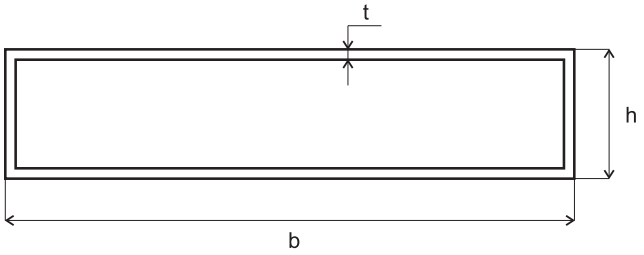

Fig. 5. Sketch of the box beam.

are clamped-free ($C-F$), clamped-supported ($C-P$) and supported-supported ($P-P$). It must be highlighted that the comparison becomes possible if both Coriolis and the Softening matrices are disregarded. In the second analysis, the structure is no longer so thin ($S = 30$) as to consider the approximations of Euler–Bernoulli model valid and, for this reason, the first order shear deformation theory is needed. The variation of the fundamental non-dimensional frequency of a cantilever Timoshenko beam with the rotating speed is shown in Table 2 and it is compared with [9]. It is important to note that no shear correction factor is used. The agreement between the two sets of results is evident, in fact, the relative error remains below 1%.

In the next example, a uniform and a tapered cantilever beam are considered, for which hub ratios are assumed to be 1 and 0, respectively. For the tapered beam, the variation of the depth of the rectangular cross-section is linear and the taper ratio, b_t/b_r is assumed to be 0.5 (see Fig. 2). For reference purposes, the results presented in [5] have been reported. As far as the uniform section is concerned, the results in Table 3 show a strong agreement between the present theory and the reference one, whereas there are some discrepancies between the two models for the tapered case especially in the computation of the fundamental frequency,

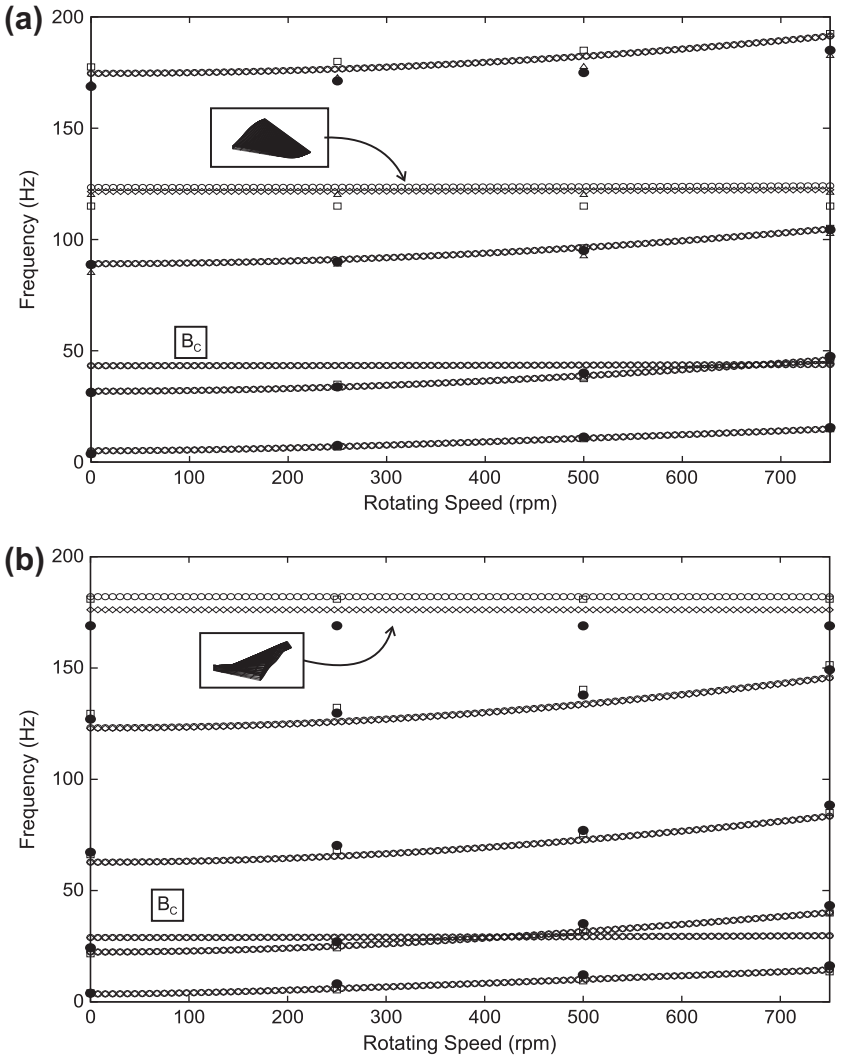

Fig. 4. Frequencies versus angular speed – "○": present (TE2), "◇": present (TE4), "□": theory [41], "△": theory [42] and "•": experimental data [42]. (a) 0°, and (b) 15°.

Table 6
Angular frequencies (rad/s) of the thin-walled box.

Ply angle	ω	TE2	TE7	2D
0°	ω_1	190.92	164.46	155.99^{F}
	ω_2	625.38	599.49	597.50^{L}
45°	ω_1	40.356	36.788	$36.083^{F/T}$
	ω_2	194.18	152.53	$145.07^{L/T}$
60°	ω_1	32.358	31.899	$31.597^{F/T}$
	ω_2	133.77	129.98	$128.47^{L/T}$
90°	ω_1	31.372	30.680	30.322^{F}
	ω_2	127.54	125.41	123.44^{L}

F: bending mode in *z* – direction.
L: bending mode in *x* – direction.
/*T*: bending/torsional coupled mode.

for which the error increases significantly with the rotating speed. The reason for this difference is due to the discretization along the longitudinal axis. In fact, in [5], the structure has been approximated by adopting a variable-order Finite Element Method conceived for tapered structures, while in contrast, in the present paper the beam is described with 40 constant cross-section beam elements where the width is uniformly decreased along the axis. Possible remedies could be to increase the number of uniform beams or to use a suitable formulation for tapered beams.

Since CUF allows us to describe the behavior of a body completely, it is possible to detect all kinds of normal modes of a rotating beam, including the chordwise motion. Consequently, in the following analysis these modes have also been studied and their frequencies are compared with those shown in [40]. As can be seen from Table 4, the results match those of the reference for all values of non-dimensional speed and hub off-set ratio. Fig. 3 shows how the frequency parameter varies with the rotating speed for both chordwise (empty dots) and flapwise (black dots) motions. In Fig. 3a, in accordance with [40], it is possible to note that the frequencies related to the stretching modes (*S*) vary with the speed in the chordwise motion while, in the flapwise case, these frequencies remain almost constant. However some remarks are needed about the occurrence of the divergence stability. In fact, in the first

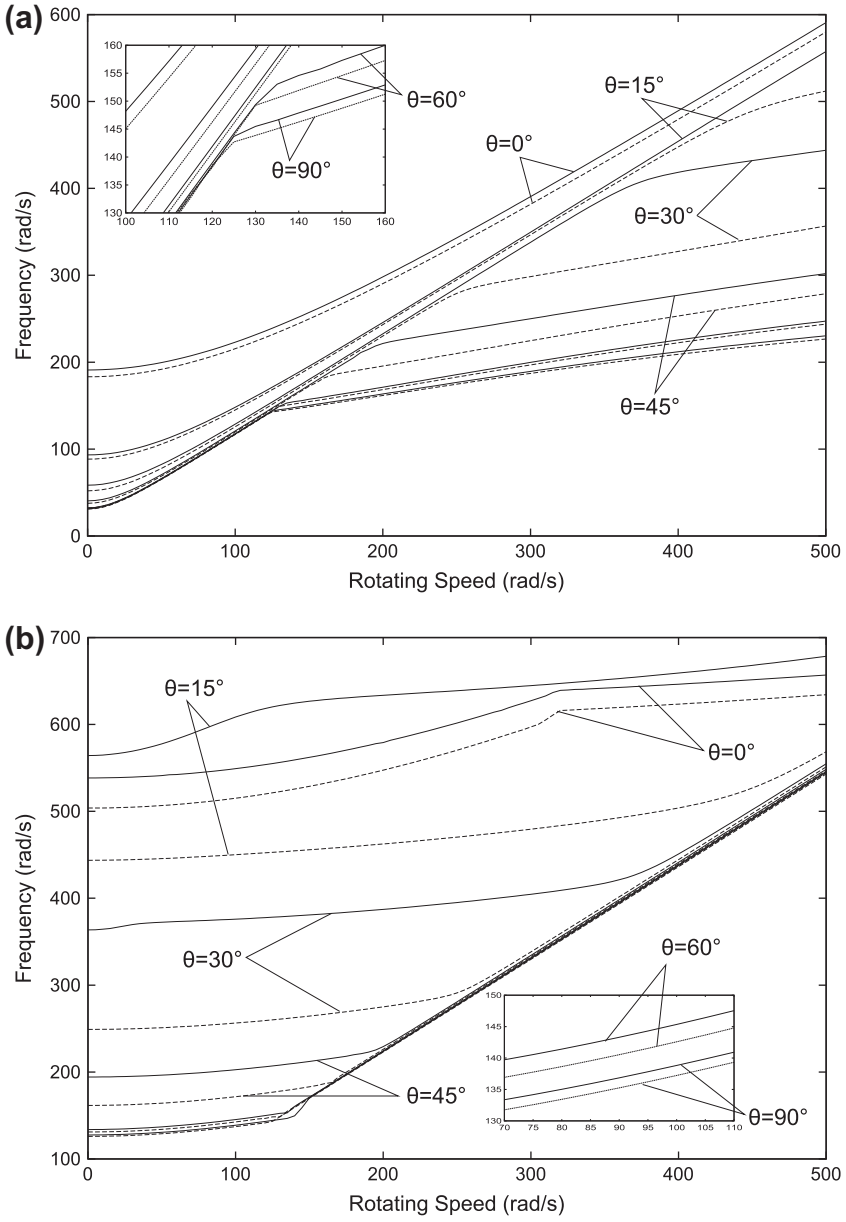

Fig. 6. First angular frequency versus rotational speed for different ply angles – "solid lines": TE2; "dotted lines":TE4. (a) ω_1 (b), and ω_2.

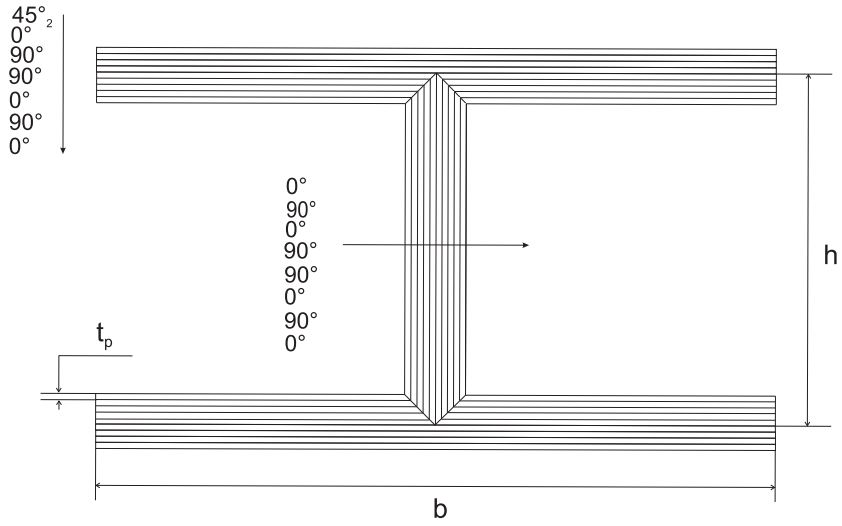

Fig. 7. Sketch of the section beam and lamination scheme.

figure, the frequency parameter related to the first bending mode in chordwise motion decreases to 0 since the non-linear term, $u_{y,y}$, has been disregarded, but if this term is included the dynamic behavior undergoes an observable change. In fact, in Fig. 3b, it is evident that the dimensionless frequencies, S_1 and S_2, start to increase with the rotating velocity and, furthermore, the divergence instability no longer occurs. Therefore, the term $u_{y,y}$ is crucial in the analysis of rotating beams especially when chordwise motion is studied.

Inasmuch as the Unified Formulation allows us to vary the kinematic theories, in these last analyses, higher-order models have been tested. The structures considered are two graphite-epoxy rectangular beams. For both beams, the width, the length and the hub off-set are assumed to be 25.4 mm and 800.01 mm and 63.5 mm, respectively. The thickness and the fiber orientations are different for the two cases and they are listed in Table 5 with the material properties. The reference solutions related to the flapwise normal modes are taken from [41], in which some experimental data presented in [42] have been reported in graphical form. As is shown in Fig. 4, the frequencies obtained with the present theory are in good agreement with the other theoretical approaches and with the experimental data. It is interesting to note that, the second-degree polynomial is enough to detect the bending modes and their related frequency values, whereas for vibration modes which are dominated by torsion, further refinements of the displacement fields are needed in order to improve the solutions. In fact by adopting the fourth-degree polynomial, the frequencies related to the normal modes shown in Fig. 4 decrease, getting close to reference values. The remaining frequencies labeled with B_C are related to chordwise modes.

In order to investigate the effects of the ply angle and the rotational speed on the frequencies of more complex and realistic structures, in the following example a thin-walled box is studied. The geometry features (see Fig. 5) and the material properties being given by:

$$E_L = 206.8 \text{ GPa} \qquad E_T = 5.17 \text{ GPa} \qquad G_{LT} = 2.55 \text{ GPa}$$
$$G_{TT} = 3.10 \text{ GPa}$$
$$\nu_{LT} = \nu_{TT} = 0.25, \qquad \rho = 1528.15 \text{ Kg/m}^3$$
$$b = 0.0508 \text{ m} \qquad c = 0.2540 \text{ m} \qquad t = 0.01016 \text{ m}$$

where L and T denote parallel and transverse directions to the fibers. The length of beam and the hub-ratio are assumed to be 2.032 m, respectively. In [13], the dependency of the first angular frequency by the rotational speed and by the ply angle orientations has been evaluated using a refined theory which takes into account some non-classical effects such as the torsion of the cross-section. Nevertheless the Coriolis terms were discarded so as to split the equations describing the flap-lag bending deformation from those related to the extension-twist motion. In the present analyses, the Coriolis matrix is included as well as the term $u_{y,y}$. In Table 6, the first two angular frequencies computed with TE2 and TE7 are compared with those obtained with shell FEM solutions, in which *QUAD*4 of *MSC NASTRAN*© have been used. The increasing number of terms in the expansions leads to a general improvement of the solution, whose accuracy strongly depends on the ply angle. Fig. 6 aims to show how the first two angular frequencies change with the rotational speed for different fiber orientations. The solid lines are obtained with the second-order expansion TE2, whereas the dotted curves with the TE4 expansion. With these two displacement models, it is possible to detect the flexural-twist coupling when the ply angles are different from 0° and 90°. By considering

Table 7
Material properties and dimensions of composite I beam in Fig. 7.

Property	Dimension
E_{11}	78.5 (Gpa)
E_{22}	5.51 (Gpa)
G_{23}	2.07 (Gpa)
G_{31}	2.07 (Gpa)
G_{12}	2.34 (Gpa)
ν_{12}	0.34
ρ	1241 (kg/m^3)
t_p	0.2286 (mm)
h	12.7 (mm)
b	25.4 (mm)
Length	844.55 (mm)

Table 8
The first two frequencies (Hz) of the composite I beam at standstill.

	TE2	TE4	TE6	Theory [18]	Exp. [18]
F	23.62	23.43	23.35	27.60	23.0
L	28.00	27.09	27.04	29.60	–

F: bending mode in z – direction.
L: bending mode in x – direction.
–: value not provided.

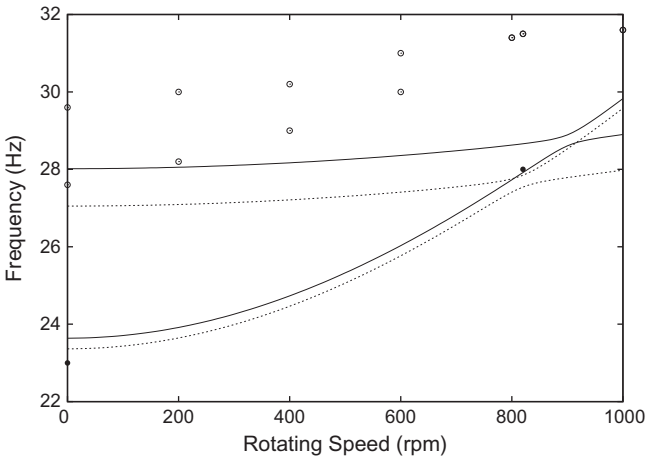

Fig. 8. Frequencies versus angular speed – "solid lines": present (TE2), "dotted lines": present (TE6), "○": theory [18] and "•": experimental data [18].

the graph 6-a it should be noted that, under a certain value of rotational speed depending on the fiber orientation, the dominant modal shape that exhibits the lowest frequency is the flapwise mode. Due to the centrifugal effect, this frequency rapidly increases until the frequency lag mode becomes the lower of the two. The same phenomenon is observed in graph 6-b for the second angular frequency but, in this case, the threshold speeds determine the interchange between the lag/torsional modal shapes and those that involve flap/extensional deformations. Moreover, for both cases, the curves computed with TE4 undergo a translation toward lower values, whereas the trends remain almost similar.

In the last analysis, a rotating composite I beam is considered. The cross-section and the lamination scheme are shown in Fig. 7, whereas the beam dimensions and the material properties are listed in Table 7. The reference solutions are taken from [18] in which a refined beam element has been developed. This analysis aims to compare the first two frequencies corresponding to the flapwise and lagging modal shapes. To this end, Table 8 shows these frequencies obtained with a number of models at standstill. As far as the flapwise mode is concerned, the TE expansions are in good agreement with the experimental data, while in contrast, they present considerable discrepancies with the solution proposed in [18]. These differences are lower for the lagging frequency. As usual, in Fig. 8, the evolutions of the frequencies with the rotational speeds are shown and, also in this case, the TE6 expansion leads to a result near the experimental reference.

6. Conclusion

In the present paper, Carrera's Unified Formulation has been developed and extended to the free vibration of rotating beams. The equations of motion were derived through Hamilton's Principle and they have been solved with the Finite Element Method. Many rotating beams were considered and, in order to assess the new theory, the results were compared with those published in the literature, where possible. The analyses have concerned isotropic, composite and non-uniform beams as well as thin-walled structures. The hierarchical property of CUF has enabled refined displacement fields with Taylor-type expansions to be obtained. The equations are written in a fully three dimensional form. The stretching and the chordwise motions are coupled by Coriolis matrix and, for this reason, the non-linear term $u_{y,y}$ in the centrifugal Stiffening matrix appears needed in order to avoid wrong predictions of instability. Furthermore, in the case of laminated beams and thin-walled boxes, the refined elements have described the evolution of the natural frequencies and relating modes with increasing accuracy with respect to the classical theories, also yielding remarkable results for shell-like deformations. In the light of these considerations, the proposed one-dimensional theory appears very appropriate for the study of rotating and spinning structures, since it combines a simple formulation with the possibility of obtaining refined models of arbitrary accuracy. The research reported in this paper is expected to stimulate further research on dynamic behavior of more complex rotating structural systems.

References

[1] Banerjee JR. Free vibration of centrifugally stiffened uniform and tapered beams using the dynamic stiffness method. J Sound Vib 2000;233:857–75.
[2] Banerjee JR, Su H, Jackson DR. Free vibration of rotating tapered beams using the dynamic stiffness method. J Sound Vib 2006;298:1034–54.
[3] Ozge Ozdemir Ozgumus, Kaya Metin O. Flapwise bending vibration analysi of doube tapered rotating Euler–Bernoulli beam by using the differential transform method. Meccanica 2006;41:661–70.
[4] Mei C. Application of differential transformation technique to free vibration analysis of a centrifugally stiffened beam. Comput Struct 2008;86:1280–4.
[5] Hodges DH, Rutkowski MJ. Free-vibration analysis of rotating beams by a variable-order finite-element method. AIAA J 1981;19:1459–66.
[6] Huang Chih Ling, Lin Wen Yi, Hsiao Kuo Mo. Free vibration analysis of rotating euler beams at high angular velocity. Comput Struct 2010;88:991–1001.
[7] Tsai Ming Hsu, Lin Wen Yi, Hsiao Kuo Mo. Investigation on steady state deformation and free vibration of a rotating inclined euer beam. Int J Mech Sci 2011;53:1050–68.
[8] Stoykov S, Ribeiro P. Vibration analysis of rotating 3d beams by *p*-version finite element method. Finite Elem Anal Des 2013;65:76–88.
[9] Lee SY, Kuo YH. Bending frequency of a rotating timoshenko beam with generally elastically restrained root. J Sound Vib 1993;162:243–50.
[10] Rao SS, Gupta RS. Finite element vibration analysis of rotating timoshenko beams. J Sound Vib 2001;242:103–24.
[11] R Banerjee J. Dynamic stiffness formulation and free vibration analysis of centrifugally stiffened timoshenko beams. J Sound Vib 2001;247:97–115.
[12] Yoo Hong Hee, Lee Seung Hyun, Shin Sang Ha. Flapwise bending vibration analysis of rotating multi-layered composite beams. J Sound Vib 2005;286:745–61.
[13] Song O, Librescu L. Structural modeling and free vibration analysis of rotating composite thin-walled beams. J Am Helicopter Soc 1997;42:358–69.
[14] Chandiramani NK, Librescu L, Shete CD. On the free-vibration of rotating composite beams using a higher-order shear formulation. Aerospace Sci Technol 2002;6:545–61.
[15] Chandiramani NK, Librescu L, Shete CD. Vibration of higher-order-shearable pretwisted rotating composite blades. Int J Mech Sci 2003;45:2017–41.
[16] Na S, Librescu L, Shim JK. Modeling and bending vibration control of nonuniform thin-walled rotating beams incorporating adaptive capabilities. Int J Mech Sci 2003;45:1347–67.
[17] Song O, Oh SY, Librescu L. Dynamic behavior of elastically taiored rotating blades modeled as pretwisted thin-walled beams and incorporating adaptive capabilities. Int J Rotating Mach 2002;8:13–25.
[18] Jung Sung Nam, Nagaraj VT, Chopra Inderjit. Refined structural dynamics model for composite rotor blades. AIAA J 2001;39:339–48.
[19] Hodges DH. Review of composite rotor blade modeling. AIAA J 1990;28:561–5.
[20] Jung Sung Nam, Nagaraj VT, Chopra Inderjit. Assessment of composite rotor blade modeling techniques. J Am Helicopter Soc 1999;44:188–205.
[21] Carrera E. Theories and finite elements for multilayered, anisotropic, composite plates and shells. Arch Comput Methods Eng 2002;9(2):87–140.
[22] Carrera E. Theories and finite elements for multilayered plates and shells: a unified compact formulation with numerical assessment and benchmarking. Arch Comput Methods Eng 2003;10(3):216–96.
[23] Carrera E, Cinefra M, Nali P. MITC technique extended to variable kinematic multilayered plate elements. Compos Struct 2010;93:1888–95.
[24] Carrera E, Miglioretti F, Petrolo M. Accuracy of refined finite elements for laminated plate analysis. Compos Struct 2011;93:1311–27.
[25] Fazzolari FA, Carrera E. Advanced variable kinematics ritz and galerkin formulations for accurate buckling and vibration analysis of anisotropic laminated composite plates. Compos Struct 2011;94:50–67.
[26] Carrera E, Giunta G, Petrolo M. Beam structures. Classical and advanced theories. Wiley; 2011.
[27] Carrera E, Giunta G. Refined beam theories based on a unified formulation. Int J Appl Mech 2010;2:117–43.
[28] Carrera E, Giunta G, Nali P, Petrolo M. Refined beam elements with arbitrary cross-section geometries. Comput Struct 2010;88(5–6):283–93. http://dx.doi.org/10.1016/j.compstruc.2009.11.002.
[29] Carrera E, Petrolo M, Zappino E. Performance of CUF approach to analyze the structural behavior of slender bodies. J Struct Eng 2012;138:285–98.
[30] Carrera E, Petrolo M, Nali P. Unified formulation applied to free vibrations finite element analysis of beams with arbitrary section. Shock Vib 2011;18(3):485–502. http://dx.doi.org/10.3233/SAV-2010-0528.

[31] Petrolo M, Zappino E, Carrera E. Refined free vibration analysis of one-dimensional structures with compact and bridge-like cross-sections. Thin–Walled Struct 2012;56:49–61. http://dx.doi.org/10.1016/j.tws.2012.03.011.
[32] Carrera E, Petrolo M, Varello A. Advanced beam formulations for free vibration analysis of conventional and joined wings. J Aerospace Eng 2012;25:282–93. http://dx.doi.org/10.1061/(ASCE)AS.1943-5525.0000130.
[33] Giunta G, Koutsawa Y, Belouettar S, Hu S. Static, free vibration and stability analysis of three-dimensional nano-beams by atomistic refined models accounting for surface free energy effect. Int J Solids Struct 2013;50:1460–72.
[34] Biscani F, Giunta G, Belouettar S, Carrera E, Hu S. Variable kinematic beam elements coupled via Arlequin method. Compos Struct 2011;93:697–708. http://dx.doi.org/10.1016/j.compstruct.2010.08.009.
[35] Carrera E, Zappino E, Filippi M. Free vibration analysis of thin–walled cylinders reinforced with longitudinal and transversal stiffeners. J Vib Acoust 2013;135. http://dx.doi.org/10.1115/1.4007559. 011019-1–011019-11.
[36] Giunta G, Crisafulli D, Belouettar S, Carrera E. Hierarchical theories for the free vibration analysis of functionally graded beams. Compos Struct 2011;94:68–74.
[37] Giunta G, Biscani F, Belouettar S, Ferreira AJM, Carrera E. Free vibration analysis of composite beams via refined theories. Composites: Part B 2013;44:540–52.
[38] Giunta G, Metla N, Koutsawa Y, Belouettar S. Free vibration and stability analysis of three-dimensional sandwich beams via hierarchical models. Composites: Part B 2013;47:5326–38.
[39] Carrera E, Filippi M, Zappino E. Laminated beam analysis by polynomial, trigonometric, exponential and zig-zag theories. Eur J Mech – A/Solids 2013;41:58–69.
[40] Chung J, Yoo HH. Dynamic analysis of a rotating cantilever beam by using the finite element method. J Sound Vib 2002;249:147–64.
[41] Hodges DH, Shang X, Cesnik CES. Finite element solution of nonlinear intrinsic equations for curved composite beams. J Am Helicopter Soc 1996;41:313–21.
[42] J Epps J, Chandra R. The natural frequencies of rotating composite beams with tip sweep. J Am Helicopter Soc 1996;41:29–36.